




High harmonics with spatially varying ellipticity

JENNIFER L. ELLIS,^{1,*} KEVIN M. DORNEY,¹ DANIEL D. HICKSTEIN,^{1,2}  NATHAN J. BROOKS,¹ CHRISTIAN GENTRY,¹ CARLOS HERNÁNDEZ-GARCÍA,³  DMITRIY ZUSIN,¹ JUSTIN M. SHAW,⁴ QUYNH L. NGUYEN,¹ CHRISTOPHER A. MANCUSO,¹ G. S. MATTHIJS JANSEN,⁵ STEFAN WITTE,⁵ HENRY C. KAPTEYN,¹  AND MARGARET M. MURNANE¹

¹JILA—Department of Physics, University of Colorado Boulder and NIST, Boulder, Colorado 80309, USA

²Time and Frequency Division, National Institute of Standards and Technology, 325 Broadway, Boulder, Colorado 80305, USA

³Grupo de Investigación en Aplicaciones del Láser y Fotónica, Departamento de Física Aplicada, University of Salamanca, Salamanca 37008, Spain

⁴Electromagnetics Division, National Institute of Standards and Technology, 325 Broadway, Boulder, Colorado 80305, USA

⁵Advanced Research Center for Nanolithography (ARCNL), Science Park 110, 1098 XG Amsterdam, The Netherlands

*Corresponding author: jennifer.ellis@colorado.edu

Received 18 January 2018; revised 13 March 2018; accepted 14 March 2018 (Doc. ID 320099); published 17 April 2018

We present a method of producing ultrashort pulses of circularly polarized extreme ultraviolet (EUV) light through high-harmonic generation (HHG). HHG is a powerful tool for generating bright laser-like beams of EUV and soft x-ray light with ultrashort pulse durations, which are important for many spectroscopic and imaging applications in the materials, chemical, and nano sciences. Historically HHG was restricted to linear polarization; however, recent advances are making it possible to precisely control the polarization state of the emitted light simply by adjusting the driving laser beams and geometry. In this work, we gain polarization control by combining two spatially separated and orthogonally linearly polarized HHG sources to produce a far-field beam with a uniform intensity distribution, but with a spatially varying ellipticity that ranges from linearly to fully circularly polarized. This spatially varying ellipticity was characterized using EUV magnetic circular dichroism, which demonstrates that a high degree of circularity is achieved, reaching almost 100% near the magnetic M-edge of cobalt. The spatial modulation of the polarization facilitates measurements of circular dichroism, enabling us to measure spectrally resolved magnetic circular dichroism without the use of an EUV spectrometer, thereby avoiding the associated losses in both flux and spatial resolution, which could enable hyperspectral imaging of chiral systems. Through numerical simulations, we also show the generality of this scheme, which can be applied with either the discrete harmonic orders generated by many-cycle pulses or the high-harmonic supercontinua generated by few-cycle driving laser pulses. Therefore, this technique provides a promising route for the production of bright isolated attosecond pulses with circular polarization that can probe ultrafast spin dynamics in materials. © 2018 Optical Society of America under the terms of the [OSA Open Access Publishing Agreement](#)

OCIS codes: (140.7240) UV, EUV, and X-ray lasers; (300.6300) Spectroscopy, Fourier transforms; (160.3820) Magneto-optical materials; (190.4160) Multiharmonic generation.

<https://doi.org/10.1364/OPTICA.5.000479>

1. INTRODUCTION

High-harmonic generation (HHG) is an extreme nonlinear optical process in which an intense femtosecond laser pulse is coherently upconverted to produce ultrashort pulses of extreme ultraviolet (EUV) and soft x-ray light [1–3]. As a unique tabletop source of ultrafast and spatially and temporally coherent beams at short wavelengths, HHG enables novel probes of atoms, molecules, and materials at their natural spatial and temporal scales. Recent advances include the use of ultrafast photoelectron spectroscopy to uncover the fastest femtosecond to attosecond charge dynamics known to date in molecules, nanoparticles, and materials [4–9], and the first subwavelength imaging at few-nanometer wavelengths [10]. Traditionally, HHG is driven by a single

linearly polarized laser, which results in linearly polarized high harmonics [11–13]. However, novel combinations of two differently polarized driving lasers can produce bright circularly polarized high harmonics [14–20]. This polarization control in HHG has made it possible to study nanoscale dynamics in magnetic, molecular, and other spin-dependent systems [17,18,21–25].

Here, we present a method of producing circularly polarized EUV light, which generates a high-harmonic beam with spatially varying ellipticity (SVE-HHG) through the coherent superposition of two spatially separated and orthogonally linearly polarized high-harmonic sources. In close analogy to a Young's double-slit experiment [26], two spatially separated high-harmonic sources diverge to overlap in the far field (Fig. 1). If the polarization

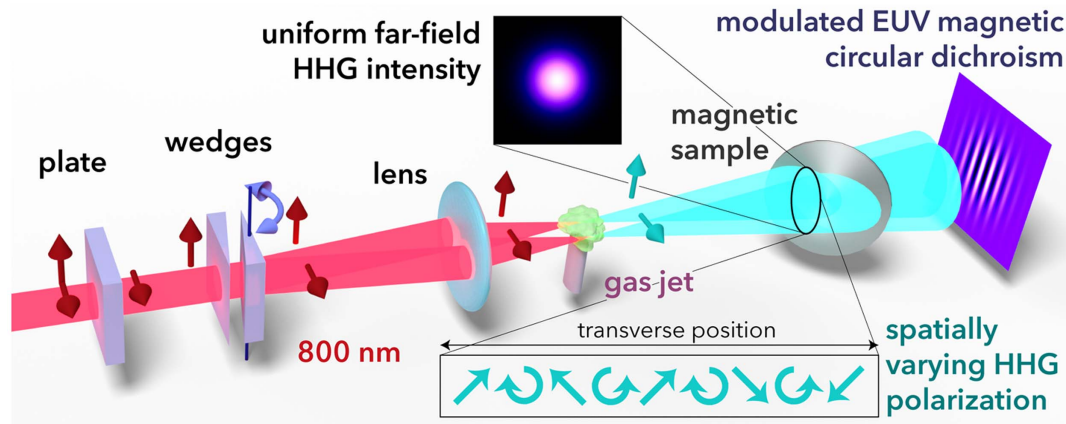


Fig. 1. Experimental setup. A common-path interferometer creates two orthogonally polarized and angularly separated beams, which are focused to two spatially separated focal spots for driving the high-harmonic generation (HHG) process in a neon gas jet. The interferometer consists of a birefringent plate and a pair of birefringent wedges (α -BBO), which split an incoming pulse into two orthogonally polarized and angularly separated pulses. The degree of angular separation is controlled by the rotation of the second wedge about the vertical axis. A lens then focuses the two orthogonally polarized beams into a gas jet and maps the angular separation into a spatial separation at the focus (exaggerated for clarity). The spatially separated focal spots each independently drive the HHG process, yielding two orthogonally polarized HHG beams, which diverge to overlap in the far field and thereby produce a far-field distribution with a spatially varying ellipticity (SVE-HHG). This ellipticity distribution is measured using the extreme ultraviolet magnetic circular dichroism (EUV MCD) response of a cobalt thin film. The fundamental is blocked with an aluminum filter (not shown) to isolate the EUV light before the magnetic sample. For clarity, idealized data are shown in the examples here.

vectors of the independent HHG sources are parallel, as in the typical Young's experiment, the far-field distribution exhibits intensity interference resulting in the classic fringe pattern [27]. However, if these two sources have orthogonal linear polarizations, then there are no interference fringes in the intensity. Instead, there is a phase interference that results in a spatially varying ellipticity [28–30]. Therefore, in the far field there is a uniform intensity profile, but the polarization in the transverse plane varies from linear to elliptical to purely circular polarization (Fig. 1). We note that this scheme was previously proposed for HHG in Zerne *et al.* [27] but to our knowledge has not been demonstrated to date.

SVE-HHG is an interesting and advantageous geometry for several reasons. First, both driving lasers are linearly polarized and independently drive the HHG process, so that both the single-atom and macroscopic physics of the HHG process are identical to that of traditional single-beam HHG. This makes SVE-HHG the first method to produce circularly polarized harmonics with the same cutoff photon energy and photon flux as linearly polarized HHG. Furthermore, when there are several harmonic orders present, the far-field polarization distribution is the coherent superposition of the spatially varying ellipticity of each individual harmonic order. Therefore, for samples that are sensitive to the polarization, a high-harmonic spectrum can be obtained via Fourier transformation of the spatial polarization pattern along the direction of the ellipticity variations. We experimentally demonstrate that this ability provides for energy-resolved measurements of circular dichroism without the use of a spectrometer, thus avoiding the associated losses and enabling spatially resolved spectroscopy of chiral systems. Finally, we show through numerical simulations that this scheme is general and can be applied to either discrete harmonic orders driven by multi-cycle pulses or high-harmonic supercontinua driven by few-cycle laser pulses. Therefore, SVE-HHG presents an exciting

route for the production of isolated attosecond pulses with circular polarization, enabling the study of the fastest known spin dynamics in magnetic materials, which can occur on femtosecond to attosecond timescales [9].

While other HHG approaches, such as the collinear or non-collinear mixing of counter-rotating beams, can also produce isolated attosecond bursts of circularly polarized EUV light [31–33], there are significant challenges in extending those techniques to the mid-infrared (IR). Mid-IR-driven HHG is advantageous because the harmonics are produced with higher photon energies and naturally emerge as isolated attosecond bursts [34,35]. However, noncollinear HHG is hampered by a finite interaction length and the need for high gas pressures to achieve reasonable conversion efficiencies [36,37], both of which decrease the achievable flux. Collinear bichromatic HHG, on the other hand, suffers from polarization degradation and eventual photon energy limits due to the spectral overlap of oppositely polarized adjacent harmonic orders [18]. In contrast, SVE-HHG can be applied with the same high conversion efficiency as single-beam HHG at any wavelength and in any geometry (gas jet, gas cell, waveguide, etc.). This makes mid-IR-driven SVE-HHG a promising route for producing bright beams of circularly polarized isolated attosecond pulses in the soft x-ray region.

2. EXPERIMENT

To experimentally implement this technique, we use a common-path interferometer to split the driving laser (KM Labs Wyvern HE, 800 nm, 45 fs, 1 kHz, 8 mJ) into two orthogonally polarized beams, which are then focused into a gas jet to drive two independent HHG sources (Fig. 1). The common-path interferometer consists of a birefringent plate [α -BBO (beta-barium borate)] with its extraordinary axis oriented vertically and a pair of birefringent wedges (α -BBO, wedge angle=100 mrad) with their

extraordinary axes oriented horizontally [38–40]. First, the birefringent plate splits the incident fundamental beam into a time-delayed and orthogonally polarized pulse pair. Following the delay plate, the beams encounter the first wedge such that one of the beams is polarized along the extraordinary axis while the other beam is polarized along the ordinary axis, which introduces an angular separation between the two orthogonally polarized beams. The second wedge compensates most of the angular separation induced by the first wedge; however, small rotations of the second wedge about the vertical axis leave a controllable amount of angular separation between the two orthogonally polarized beams. Additionally, since the extraordinary axis of the delay plate is orthogonal to those of the wedges, the time delay between the two fundamental pulses can be precisely compensated by the degree of insertion of the second wedge. Finally, a focusing lens ($f = 25$ cm, waist ~ 40 μm) is positioned after the interferometer such that the angular separation between the two beams (~ 0.2 mrad) is mapped to a spatial separation (~ 100 μm) at the focus (i.e., the second wedge is at the back focal plane of the lens). Each linearly polarized beam independently drives the HHG process in a neon gas jet, producing two spatially separated and orthogonally polarized HHG sources (Fig. 1). These two high-harmonic beams diverge and overlap in the far field, thereby producing a uniform intensity distribution and a sinusoidally spatially varying ellipticity.

3. CHARACTERIZATION OF FAR-FIELD POLARIZATION

We confirm the spatially varying ellipticity of the SVE-HHG scheme through EUV magnetic circular dichroism (EUV MCD), in which the magnetic state of a material is probed by the dichroic absorption of circularly polarized light (Fig. 1) [41]. The helicity-dependent absorption of light by magnetic materials varies linearly with the degree of circularity of the illuminating field, i.e., with the ratio of the Stokes parameters, S_3/S_0 [42,43]. Therefore, EUV MCD provides a rigorous characterization of the polarization state of this source. We perform EUV MCD measurements on a 20-nm-thick cobalt film, which is supported on 200 nm of aluminum. An electromagnet magnetizes the cobalt in the plane of the thin film, which is oriented at 45 degrees with respect to the direction of propagation of the harmonic beam. This geometry results in a reasonable projection of the in-plane magnetization vector along the spin-angular momentum vector of the incident light. We compare the transmitted EUV intensity for opposite magnetizations of the film ($I_{+,-}$) and quantify the dichroism signal via the magnetic asymmetry, $A = (I_+ - I_-)/(I_+ + I_-)$ [42]. Placing a curved grating (Hitachi 001-0266) after the magnetic sample spectrally resolves the harmonics in one dimension while preserving spatial resolution in the dimension of the polarization modulations, thereby enabling the measurement of the spatially resolved magnetic asymmetry for each harmonic order individually.

While the transmitted intensity does not directly show any interference due to the orthogonal polarization of the two harmonic sources [Fig. 2(a)], the spatially varying ellipticity is revealed upon subtraction of the transmitted intensity for the two opposite magnetizations of the cobalt film [Fig. 2(b)]. This polarization grating manifests as a sinusoidal variation in the magnetic asymmetry spatially along the beam profile, which is visible in several harmonic orders. Since the film is uniformly

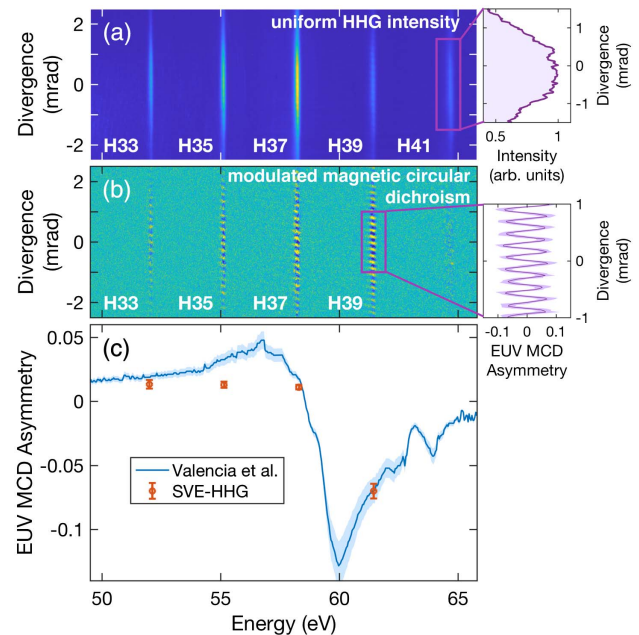


Fig. 2. Spatially varying ellipticity in SVE-HHG is characterized via EUV magnetic circular dichroism (EUV MCD). (a) The spectrally resolved intensity of harmonics transmitted through a uniformly magnetized 20-nm-thick cobalt thin film shows a spatially uniform intensity profile. (b) Subtraction of the harmonic intensity transmitted through the cobalt thin film with two opposite magnetizations shows a sinusoidal spatial variation vertically along each harmonic profile. This is due to the differential absorption in MCD, which reveals the spatially varying ellipticity across the high-harmonic beam profile. (c) The amplitude of our measured EUV MCD asymmetry (red circles) is compared with values in the literature (Valencia *et al.* [44]) for the magnetic asymmetry expected from a 20-nm-thick cobalt film [44] (blue line with errors represented by the shaded region) to determine the maximum ellipticity present in the far-field polarization distribution. The close agreement with previous measurements indicates a high degree of circularity. The errors on the SVE-HHG data points represent the statistical errors in the fitting procedure and therefore do not capture any systematic effects. We estimate that the systematic errors present are smaller than the statistical ones shown here.

magnetized, this variation in the asymmetry is due to the spatially varying ellipticity of the high-harmonic light, where zero asymmetry indicates linear polarization and positive or negative asymmetry corresponds to either right or left circular polarization, depending on the sign of the MCD response of the material. Therefore, the amplitude of the sinusoidal variation in the magnetic asymmetry is directly related to the maximum ellipticity present in the high-harmonic polarization distribution [Fig. 2(b) inset]. Additionally, the relative phase of the sinusoidally varying asymmetry between harmonic orders indicates the relative sign of the EUV MCD (see Supplement 1).

Comparison with literature values for the magnetic asymmetry of cobalt films [44] indicates that the degree of circularity attained is high [Fig. 2(c)], approaching 100% near the magnetic M-edge of cobalt (see Supplement 1). There are some discrepancies in the measured asymmetry at the harmonic orders below the M-edge, especially for H35 at ~ 55 eV. However, this difference is likely due to differences in the sample preparation techniques used here versus those in Valencia *et al.*, which could

modify the magneto-optical constants being probed. These small modifications would have larger ramifications away from the M-edge, where the MCD effect is small. While it is possible that this deviation is due to a lower degree of circularity for H35, it is physically unlikely that the polarization quality would vary so much between adjacent harmonic orders. This is because no such decreased circularity for a single harmonic order was seen in the numerical simulations presented below, and there is no resonance in neon or any other factors that we can identify that would only affect H35.

To confirm these results, we repeated the measurement with an unmagnetized sample and observed no modulations in the asymmetry, indicating that these sinusoidal variations are indeed due to EUV MCD in the cobalt film, thus confirming the spatially varying ellipticity of the high harmonics (see Supplement 1). We note that reflection off the grating does have polarization dependence, so that after the grating the circularity of the harmonics is diminished. However, the magnetic sample is upstream from the grating, so this does not affect the MCD measurement. This polarization dependence can impart a fringe structure on the reflected harmonics depending on the orientation of the polarization of the linearly polarized regions, which is useful for alignment purposes but is minimized when taking MCD measurements (by rotating the linearly polarized regions to be an equal mixture of *s* and *p* polarization).

4. SPATIALLY RESOLVED MAGNETIC SPECTROSCOPY

After characterizing the spatially varying ellipticity and high degree of circularity obtained with SVE-HHG, we investigated this scheme's applicability for spatially resolved dichroic spectroscopy. Spatially resolved spectroscopy is possible in SVE-HHG because the far-field polarization pattern is a coherent superposition of the sinusoidal ellipticity variation of each harmonic order present, the spatial frequency of which depends on the harmonic wavelength. Consequently, a Fourier transform of the spatially varying dichroism signal recovers the harmonic spectrum without the need for dispersive optics [45], thereby avoiding the associated losses in both flux and spatial resolution.

To demonstrate this unique capability, we measure the fully spatially resolved EUV MCD response of the same cobalt thin film, simply by propagating the harmonic beam directly from the sample to the CCD without using a grating [Fig. 3(a)]. Again, the magnetic asymmetry shows clear spatial variations [Fig. 3(b)], which, in this case, are the result of the coherent superposition of the sinusoidal ellipticity variations of the four harmonic orders contributing to the MCD signal [Fig. 2(b)]. A Fourier transform of the magnetic asymmetry along the plane of ellipticity variation recovers the high-harmonic spectrum transmitted through the sample, multiplied by the energy-dependent magnetic asymmetry [Fig. 3(c); see Supplement 1]. Therefore, by independently measuring the spectral weights of the individual harmonic orders transmitted through the sample, we can extract the energy-dependent EUV MCD asymmetry. This measurement is in excellent agreement with the MCD values obtained using a spectrometer to spectrally disperse the harmonic orders [Fig. 3(d)].

In this work, we measured the spectral weights of the transmitted harmonic orders using a grating. We only measured the

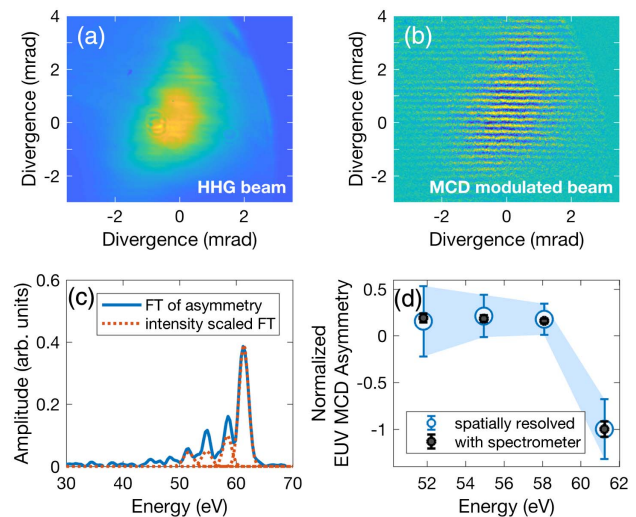


Fig. 3. Energy-resolved EUV MCD without the use of a spectrometer. (a) Intensity profile of the high-harmonic beam transmitted through a thin cobalt film (20 nm). (b) Subtraction of the transmission through the two opposite magnetizations shows the coherent superposition of the spatially varying ellipticity of several harmonic orders contributing to the MCD signal. (c) A Fourier transform (FT) of the spatially varying EUV MCD asymmetry recovers the transmitted harmonic spectrum multiplied by the energy-dependent dichroic response of the material (solid blue curve). Therefore, scaling by the transmitted spectral weights of the individual harmonic orders isolates the material's dichroic response (dotted red curve). (d) The relative EUV MCD asymmetry obtained using a spatial FT to separate the spectral content (blue) is in excellent agreement with the values obtained by spectrally dispersing the harmonic orders with a spectrometer (black), indicating that this scheme recovers the spectrally resolved MCD response of magnetic materials without the need for a grating. The blue shaded region indicates the standard deviation in the FT-recovered MCD asymmetry.

spectral region near the cobalt M-edge, instead of the entire high-harmonic spectrum, so that only the relative EUV MCD response between harmonic orders could be calculated. However, measuring the entire transmitted spectrum does enable the recovery of the absolute MCD response (see Supplement 1). An alternative to using a grating to measure the transmitted HHG spectrum is to instead characterize the harmonics by making the polarization of the two focal spots parallel, which results in an intensity interference that similarly contains the spectral weights.

5. NUMERICAL SIMULATIONS

We further support these experimental characterizations with theoretical simulations of SVE-HHG including propagation [46] (see Supplement 1 for details). In the simulations, as in the experiment, two independent orthogonally polarized focal spots (800 nm, 10.6 fs pulse duration) drive the HHG process in neon gas, and the single-atom response is propagated to the far field, where the beams overlap. The resulting polarization distribution exhibits a sinusoidal spatial variation in the degree of circularity for each harmonic order, which can be seen by isolating the projection of the polarization distribution into pure right circular polarization [Fig. 4(a)]. The projection along left circular polarization is identical except for being spatially phase shifted by π .

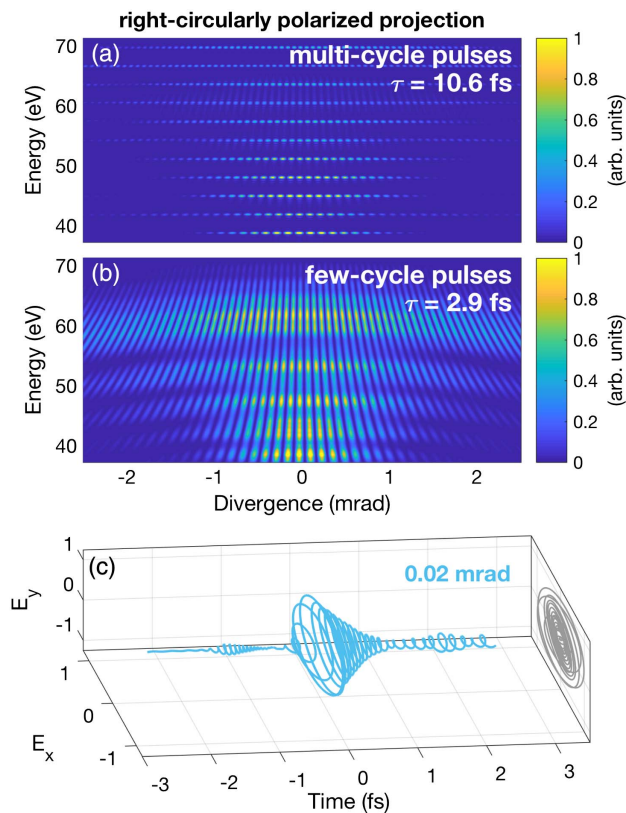


Fig. 4. Numerical simulations of SVE-HHG visualized by taking the projection of the far-field polarization distribution along pure right-circular polarization. (a) For multicycle pulses, the HHG emission is spectrally resolved into well-separated harmonic orders, which each exhibit a polarization modulation with a spatial frequency that depends on the harmonic order; (b) for near-single-cycle pulses, an HHG supercontinuum is produced. However, every energy level still exhibits sinusoidally varying ellipticity with a well-defined spatial frequency that increases with increasing photon energy. (c) This HHG supercontinuum corresponds to an isolated attosecond pulse in the time domain, which is either circularly, elliptically, or linearly polarized depending on divergence angle (± 0.02 mrad for circular; see Supplement 1).

After confirming that SVE-HHG does indeed produce a spatially varying ellipticity that reaches pure circular polarization, we performed similar simulations with near-single-cycle pulses [2.9 fs; Fig. 4(b)]. Here a quasi-supercontinuum is generated instead of individual harmonic orders, but the unique polarization properties of this source are maintained. This makes SVE-HHG a promising route for producing bright isolated attosecond pulses with circular polarization [Fig. 4(c); see Supplement 1]. While it is potentially possible to make circularly polarized isolated attosecond pulses via either collinear [31] or noncollinear [32,33] mixing of two counter-rotating driving lasers, these methods suffer from a decrease in flux due to either single-atom or macroscopic effects. Fortunately, in SVE-HHG the HHG process itself is identical to single-beam HHG, so the attainable fluxes and cutoff photon energies are just as high as in traditional single-beam HHG. Additionally, since the SVE-HHG supercontinuum still exhibits a clear sinusoidal polarization modulation at every energy level, a spatial Fourier transform will still be able to recover the spectral content. Therefore, SVE-HHG can be extended to HHG supercontinua to measure spatially resolved EUV MCD with greater

energy resolution than that attainable with spectrally isolated high harmonics. In the supercontinuum case, the energy resolution is limited only by the geometry of both the source and sample and the subsequent energy resolution obtained from the spatial Fourier transform. In the present work, we achieved an experimental energy resolution of ~ 1.3 eV, which was adequate to distinguish the well-separated high-harmonic orders (~ 3 eV separation). This energy resolution can be increased by both moving the focal spots farther apart to increase the fringe density and increasing the angular range over which light is detected. Through these numerical simulations, we have demonstrated good agreement between the true spectrum and the spectrum obtained via spatial Fourier transform. However, we find small discrepancies between the two due to the nonuniform intensity distribution across the Gaussian focal spots and the resulting transverse-phase-matching conditions [47,48]. These discrepancies could therefore be mitigated by using flat-top beams to drive the HHG process (see Supplement 1).

6. DISCUSSION AND CONCLUSIONS

In conclusion, we experimentally and theoretically demonstrate that two spatially separated and orthogonally linearly polarized harmonic sources can be combined to produce a high-harmonic beam with sinusoidally spatially varying ellipticity in the far field. We found that this polarization distribution exhibits regions with a high degree of circularity, thereby making SVE-HHG a useful technique for studying circular dichroism in the EUV. Additionally, numerical simulations show that SVE-HHG is compatible with short-pulse driving lasers, enabling the production of isolated attosecond pulses with circular polarization to probe the fastest chiral processes known to date [9]. Indeed, SVE-HHG is a promising route for producing circularly polarized isolated attosecond pulses with mid-IR driven HHG, since it does not suffer from the unfavorable scalings that hinder the extension of other methods of circularly polarized HHG into the mid-IR. Furthermore, we have shown that SVE-HHG enables spatially resolved spectroscopy of dichroic samples. This capability arises because energy resolution can be recovered through the spatial variation in the ellipticity of the source itself without the use of a spectrometer, thereby allowing us to obtain spectral resolution without sacrificing spatial resolution. One limitation of SVE-HHG is that the attainable HHG spot sizes are larger than those achievable in other methods of circularly polarized HHG. Therefore, although the flux is comparable to that of single-beam HHG, the fluence on a sample may be lower. This increase in spot size arises because in SVE-HHG the source cannot be imaged to the sample without losing the SVE present in the far-field beam. However, it is possible to instead image the far-field beam to a sample with a large demagnification to maintain the polarization properties upon focusing. While this will indeed result in larger spot sizes than if the source itself could be imaged, there are many experiments that do not require the smallest spot sizes or highest fluences in which SVE-HHG would be applicable. Another situation where other methods of circularly polarized HHG are better suited than SVE-HHG is when a pure beam of a single polarization state is required. While there are some experiments where a pure circularly polarized beam is necessary, such as photoelectron circular dichroism studies, there are also many situations where spatially varying ellipticity is acceptable or even advantageous.

Looking forward, an exciting extension of this technique is to combine it with Fourier transform spectroscopy by controlling the

time delay between the two high-harmonic sources [34,38,49–52]. In that case, the energy resolution achievable would be limited by the range in time that is scanned instead of the source and sample geometry, enabling higher energy resolution than can feasibly be obtained with the current scheme. This increase in energy resolution via Fourier transform spectroscopy is especially useful in combination with short-pulse driving lasers to easily exploit the energetically dense supercontinuum spectrum. Additionally, controlling the time delay between the two sources is advantageous because it entails EUV MCD measurements through changing the local helicity of the light, instead of flipping the magnetization state of the sample. This capability enables the study of dichroism in samples that are not uniformly magnetized, such as magnetic domains and grain boundaries, or high-coercivity samples that cannot be magnetized along an external magnetic field. Finally, we note that when the time delay is scanned, SVE-HHG is, in principle, compatible with coherent diffractive imaging techniques, enabling nanoscale hyperspectral magnetic imaging.

Note: Certain commercial equipment, instruments, or materials are identified in this paper in order to specify the experimental procedure adequately. Such identification is not intended to imply recommendation or endorsement by the National Institute of Standards and Technology, nor is it intended to imply that the materials or equipment identified are necessarily the best available for the purpose.

Funding. U.S. Department of Energy (DOE), Office of Basic Energy Sciences (BES) (DE-FG02-99ER14982, DE-SC0002002); National Science Foundation (NSF) (DGE-1144083); Fundación BBVA; Ministerio de Economía y Competitividad (MINECO) (FIS2016-75652-P); Nederlandse Organisatie voor Wetenschappelijk Onderzoek (NWO); Barcelona Supercomputing Center - Centro Nacional de Supercomputación (BSC-CSN) (RES-FI-2017-3-0004).

Acknowledgment. This work was done at JILA. The authors gratefully acknowledge support from the Department of Energy (DOE) Office of Basic Energy Sciences (AMOS program) for the light science aspect of this work, and also thank the DOE Office of Basic Energy Sciences X-Ray Scattering Program for the magnetic spectroscopy measurements performed for this work. J. E., N. B., and Q. N. acknowledge support from the National Science Foundation Graduate Research Fellowship. C. H.-G. acknowledges a 2017 Leonardo Grant for Researchers and Cultural Creators from the BBVA Foundation and support from the Ministerio de Economía y Competitividad (MINECO). S. W. and M. J. acknowledge support from the Netherlands Organisation for Scientific Research (NWO). C. H.-G. thankfully acknowledges the computer resources at MareNostrum and the technical support provided by Barcelona Supercomputing Center—Centro Nacional de Supercomputación. M. M. and H. K. have a financial interest in KMLabs.

See [Supplement 1](#) for supporting content.

REFERENCES

1. A. McPherson, G. Gibson, H. Jara, U. Johann, T. S. Luk, I. A. McIntyre, K. Boyer, and C. K. Rhodes, "Studies of multiphoton production of vacuum-ultraviolet radiation in the rare gases," *J. Opt. Soc. Am. B* **4**, 595 (1987).
2. M. Ferray, A. L'Huillier, X. F. Li, L. A. Lompre, G. Mainfray, and C. Manus, "Multiple-harmonic conversion of 1064 nm radiation in rare gases," *J. Phys. B* **21**, L31–L35 (1988).
3. A. Rundquist, C. G. Durfee, Z. Chang, C. Herne, S. Backus, M. M. Murnane, and H. C. Kapteyn, "Phase-matched generation of coherent soft x-rays," *Science* **280**, 1412–1415 (1998).
4. M. Schultze, M. Fiess, N. Karpowicz, J. Gagnon, M. Korbman, M. Hofstetter, S. Neppl, A. L. Cavalieri, Y. Komminos, T. Mercouris, C. A. Nicolaides, R. Pazourek, S. Nagele, J. Feist, J. Burgdörfer, A. M. Azzeer, R. Ernstorfer, R. Kienberger, U. Kleineberg, E. Goulielmakis, F. Krausz, and V. S. Yakovlev, "Delay in photoemission," *Science* **328**, 1658–1662 (2010).
5. M. Huppert, I. Jordan, D. Baykusheva, A. von Conta, and H. J. Wörner, "Attosecond delays in molecular photoionization," *Phys. Rev. Lett.* **117**, 093001 (2016).
6. F. Süßmann and M. F. Kling, "Attosecond nanoplasmonic streaking of localized fields near metal nanospheres," *Phys. Rev. B* **84**, 121406 (2011).
7. L. Seiffert, Q. Liu, S. Zherebtsov, A. Trabattoni, P. Rupp, M. C. Castrovilli, M. Galli, F. Süßmann, K. Wintersperger, J. Stierle, G. Sansone, L. Poletto, F. Frassetto, I. Halfpap, V. Mondes, C. Graf, E. Rühl, F. Krausz, M. Nisoli, T. Fennel, F. Calegari, and M. F. Kling, "Attosecond chronoscopy of electron scattering in dielectric nanoparticles," *Nat. Phys.* **13**, 766–770 (2017).
8. Z. Tao, C. Chen, T. Szilvási, M. Keller, M. Mavrikakis, H. Kapteyn, and M. Murnane, "Direct time-domain observation of attosecond final-state lifetimes in photoemission from solids," *Science* **353**, 62–67 (2016).
9. C. Chen, Z. Tao, A. Carr, P. Matyba, T. Szilvási, S. Emmerich, M. Piecuch, M. Keller, D. Zusin, S. Eich, M. Rollinger, W. You, S. Mathias, U. Thumm, M. Mavrikakis, M. Aeschlimann, P. M. Oppeneer, H. Kapteyn, and M. Murnane, "Distinguishing attosecond electron-electron scattering and screening in transition metals," *Proc. Natl. Acad. Sci. USA* **114**, E5300–E5307 (2017).
10. D. F. Gardner, M. Tanksalvala, E. R. Shanblatt, X. Zhang, B. R. Galloway, C. L. Porter, R. Karl, Jr., C. Bevis, D. E. Adams, H. C. Kapteyn, M. M. Murnane, and G. F. Mancini, "Subwavelength coherent imaging of periodic samples using a 13.5 nm tabletop high-harmonic light source," *Nat. Photonics* **11**, 259–263 (2017).
11. P. B. Corkum, "Plasma perspective on strong field multiphoton ionization," *Phys. Rev. Lett.* **71**, 1994–1997 (1993).
12. K. S. Budil, P. Salières, A. L'Huillier, T. Ditmire, and M. D. Perry, "Influence of ellipticity on harmonic generation," *Phys. Rev. A* **48**, R3437–R3440 (1993).
13. P. Dietrich, N. H. Burnett, M. Ivanov, and P. B. Corkum, "High-harmonic generation and correlated two-electron multiphoton ionization with elliptically polarized light," *Phys. Rev. A* **50**, R3585–R3588 (1994).
14. H. Eichmann, A. Egbert, S. Nolte, C. Momma, B. Wellegehausen, W. Becker, S. Long, and J. K. McIver, "Polarization-dependent high-order two-color mixing," *Phys. Rev. A* **51**, R3414–R3417 (1995).
15. D. B. Milošević and W. Becker, "Attosecond pulse trains with unusual nonlinear polarization," *Phys. Rev. A* **62**, 011403 (2000).
16. A. Fleischer, O. Kfir, T. Diskin, P. Sidorenko, and O. Cohen, "Spin angular momentum and tunable polarization in high-harmonic generation," *Nat. Photonics* **8**, 543–549 (2014).
17. O. Kfir, P. Grychtol, E. Turgut, R. Knut, D. Zusin, D. Popmintchev, T. Popmintchev, H. Nembach, J. M. Shaw, A. Fleischer, H. Kapteyn, M. Murnane, and O. Cohen, "Generation of bright phase-matched circularly-polarized extreme ultraviolet high harmonics," *Nat. Photonics* **9**, 99–105 (2014).
18. T. Fan, P. Grychtol, R. Knut, C. Hernández-García, D. D. Hickstein, D. Zusin, C. Gentry, F. J. Dollar, C. A. Mancuso, C. W. Hogle, O. Kfir, D. Legut, K. Carva, J. L. Ellis, K. M. Dorney, C. Chen, O. G. Shpyrko, E. E. Fullerton, O. Cohen, P. M. Oppeneer, D. B. Milošević, A. Becker, A. A. Jarón-Becker, T. Popmintchev, M. M. Murnane, and H. C. Kapteyn, "Bright circularly polarized soft x-ray high harmonics for x-ray magnetic circular dichroism," *Proc. Natl. Acad. Sci. USA* **112**, 14206–14211 (2015).
19. D. D. Hickstein, F. J. Dollar, P. Grychtol, J. L. Ellis, R. Knut, C. Hernández-García, D. Zusin, C. Gentry, J. M. Shaw, T. Fan, K. M. Dorney, A. Becker, A. Jarón-Becker, H. C. Kapteyn, M. M. Murnane, and C. G. Durfee, "Non-collinear generation of angularly isolated circularly polarized high harmonics," *Nat. Photonics* **9**, 743–750 (2015).

20. G. Lambert, B. Vodungbo, J. Gautier, B. Mahieu, V. Malka, S. Sebban, P. Zeitoun, J. Luning, J. Perron, A. Andreev, S. Stremoukhov, F. Ardana-Lamas, A. Dax, C. P. Hauri, A. Sardinha, and M. Fajardo, "Towards enabling femtosecond helicity-dependent spectroscopy with high-harmonic sources," *Nat. Commun.* **6**, 6167 (2015).
21. N. Böwering, T. Lischke, B. Schmidtke, N. Müller, T. Khalil, and U. Heinzmann, "Asymmetry in photoelectron emission from chiral molecules induced by circularly polarized light," *Phys. Rev. Lett.* **86**, 1187–1190 (2001).
22. F. Gaie-Levrel, G. A. Garcia, M. Schwell, and L. Nahon, "VUV state-selected photoionization of thermally-desorbed biomolecules by coupling an aerosol source to an imaging photoelectron/photoion coincidence spectrometer: case of the amino acids tryptophan and phenylalanine," *Phys. Chem. Chem. Phys.* **13**, 7024–7036 (2011).
23. A. Ferré, C. Handschin, M. Dumergue, F. Burgy, A. Comby, D. Descamps, B. Fabre, G. A. Garcia, R. Généaux, L. Merceron, E. Mével, L. Nahon, S. Petit, B. Pons, D. Staedter, S. Weber, T. Ruchon, V. Blanchet, and Y. Mairesse, "A table-top ultrashort light source in the extreme ultraviolet for circular dichroism experiments," *Nat. Photonics* **9**, 93–98 (2015).
24. S. Beaulieu, A. Comby, B. Fabre, D. Descamps, A. Ferré, G. Garcia, R. Généaux, F. Légaré, L. Nahon, S. Petit, T. Ruchon, B. Pons, V. Blanchet, and Y. Mairesse, "Probing ultrafast dynamics of chiral molecules using time-resolved photoelectron circular dichroism," *Faraday Discuss* **194**, 325–348 (2016).
25. E. Beaurepaire, J.-C. Merle, A. Daunois, and J.-Y. Bigot, "Ultrafast spin dynamics in ferromagnetic nickel," *Phys. Rev. Lett.* **76**, 4250–4253 (1996).
26. T. Young, "The Bakerian lecture: on the theory of light and colours," *Philos. Trans. R. Soc. Lond.* **92**, 12–48 (1802).
27. R. Zerme, C. Altucci, M. Bellini, M. B. Gaarde, T. W. Hänsch, A. L'Huillier, C. Lyngå, and C.-G. Wahlström, "Phase-locked high-order harmonic sources," *Phys. Rev. Lett.* **79**, 1006–1009 (1997).
28. W. R. Mellen, "Interference of linearly polarized light with perpendicular polarizations," *Am. J. Phys.* **30**, 772 (1962).
29. R. Hanau, "Interference of linearly polarized light with perpendicular polarizations," *Am. J. Phys.* **31**, 303–304 (1963).
30. E. Collett, "Mathematical formulation of the interference laws of Fresnel and Arago," *Am. J. Phys.* **39**, 1483–1495 (1971).
31. K. M. Dorney, J. L. Ellis, C. Hernández-García, D. D. Hickstein, C. A. Mancuso, N. Brooks, T. Fan, G. Fan, D. Zusin, C. Gentry, P. Grychtol, H. C. Kapteyn, and M. M. Murnane, "Helicity-selective enhancement and polarization control of attosecond high harmonic waveforms driven by bichromatic circularly polarized laser fields," *Phys. Rev. Lett.* **119**, 063201 (2017).
32. C. Hernández-García, C. G. Durfee, D. D. Hickstein, T. Popmintchev, A. Meier, M. M. Murnane, H. C. Kapteyn, I. J. Sola, A. Jaron-Becker, and A. Becker, "Schemes for generation of isolated attosecond pulses of pure circular polarization," *Phys. Rev. A* **93**, 043855 (2016).
33. P.-C. Huang, C.-H. Lu, C. Hernandez-Garcia, R.-T. Huang, P.-S. Wu, D. D. Hickstein, D. Thrasher, J. L. Ellis, A. H. Kung, S.-D. Yang, A. Jaron-Becker, A. Becker, H. C. Kapteyn, M. M. Murnane, C. G. Durfee, and M.-C. Chen, "Isolated, circularly polarized, attosecond pulse generation," in *Conference on Lasers and Electro-Optics* (2016), paper JTh4A.7.
34. M.-C. Chen, C. Mancuso, C. Hernández-García, F. Dollar, B. Galloway, D. Popmintchev, P.-C. Huang, B. Walker, L. Plaja, A. A. Jaron-Becker, A. Becker, M. M. Murnane, H. C. Kapteyn, and T. Popmintchev, "Generation of bright isolated attosecond soft X-ray pulses driven by multicycle midinfrared lasers," *Proc. Natl. Acad. Sci. USA* **111**, E2361–E2367 (2014).
35. S. M. Teichmann, F. Silva, S. L. Cousin, M. Hemmer, and J. Biegert, "0.5-keV soft x-ray attosecond continua," *Nat. Commun.* **7**, 11493 (2016).
36. J. L. Ellis, K. M. Dorney, C. G. Durfee, C. Hernández-García, F. Dollar, C. A. Mancuso, T. Fan, D. Zusin, C. Gentry, P. Grychtol, H. C. Kapteyn, M. M. Murnane, and D. D. Hickstein, "Phase matching of noncollinear sum and difference frequency high harmonic generation above and below the critical ionization level," *Opt. Express* **25**, 10126–10144 (2017).
37. C. M. Heyl, P. Rudawski, F. Brizuela, S. N. Bengtsson, J. Mauritsson, and A. L'Huillier, "Macroscopic effects in noncollinear high-order harmonic generation," *Phys. Rev. Lett.* **112**, 143902 (2014).
38. G. S. M. Jansen, D. Rudolf, L. Freisem, K. S. E. Eikema, and S. Witte, "Spatially resolved Fourier transform spectroscopy in the extreme ultraviolet," *Optica* **3**, 1122–1125 (2016).
39. D. Brida, C. Manzoni, and G. Cerullo, "Phase-locked pulses for two-dimensional spectroscopy by a birefringent delay line," *Opt. Lett.* **37**, 3027–3029 (2012).
40. A. Oriana, J. Réhault, F. Preda, D. Polli, and G. Cerullo, "Scanning Fourier transform spectrometer in the visible range based on birefringent wedges," *J. Opt. Soc. Am. A* **33**, 1415–1420 (2016).
41. P. J. Stephens, "Magnetic circular dichroism," *Ann. Rev. Phys. Chem.* **25**, 201–232 (1974).
42. P. M. Oppeneer, "Magneto-optical Kerr spectra," in *Handbook of Magnetic Materials*, K. H. J. Buschow, ed. (Elsevier, 2001), Vol. **13**, pp. 229–422.
43. J. Stohr and H. C. Siegmann, *Magnetism: from Fundamentals to Nanoscale Dynamics*, Vol. 152 of Springer Series in Solid-State Sciences (Springer, 2006).
44. S. Valencia, A. Gaupp, W. Gudat, H.-C. Mertins, P. M. Oppeneer, D. Abramsohn, and C. M. Schneider, "Faraday rotation spectra at shallow core levels: 3p edges of Fe, Co, and Ni," *New J. Phys.* **8**, 254 (2006).
45. M. J. Padgett and A. R. Harvey, "A static Fourier-transform spectrometer based on Wollaston prisms," *Rev. Sci. Instrum.* **66**, 2807–2811 (1995).
46. C. Hernández-García, J. A. Pérez-Hernández, J. Ramos, E. C. Jarque, L. Roso, and L. Plaja, "High-order harmonic propagation in gases within the discrete dipole approximation," *Phys. Rev. A* **82**, 033432 (2010).
47. C. Hernández-García, I. J. Sola, and L. Plaja, "Signature of the transversal coherence length in high-order harmonic generation," *Phys. Rev. A* **88**, 043848 (2013).
48. F. Catoire, A. Ferré, O. Hort, A. Dubrouil, L. Quintard, D. Descamps, S. Petit, F. Burgy, E. Mével, Y. Mairesse, and E. Constant, "Complex structure of spatially resolved high-order-harmonic spectra," *Phys. Rev. A* **94**, 063401 (2016).
49. M. Kovačev, S. V. Fomichev, E. Priori, Y. Mairesse, H. Merdji, P. Monchicourt, P. Breger, J. Norin, A. Persson, A. L'Huillier, C.-G. Wahlström, B. Carré, and P. Salières, "Extreme ultraviolet Fourier-transform spectroscopy with high order harmonics," *Phys. Rev. Lett.* **95**, 223903 (2005).
50. S. Witte, V. T. Tenner, D. W. Noom, and K. S. Eikema, "Lensless diffractive imaging with ultra-broadband table-top sources: from infrared to extreme-ultraviolet wavelengths," *Light Sci. Appl.* **3**, e163 (2014).
51. Y. Meng, C. Zhang, C. Marceau, A. Y. Naumov, P. B. Corkum, and D. M. Villeneuve, "Octave-spanning hyperspectral coherent diffractive imaging in the extreme ultraviolet range," *Opt. Express* **23**, 28960–28969 (2015).
52. Y. Nabekawa, T. Shimizu, Y. Furukawa, E. J. Takahashi, and K. Midorikawa, "Interferometry of attosecond pulse trains in the extreme ultraviolet wavelength region," *Phys. Rev. Lett.* **102**, 213904 (2009).